Palaeogeography, Palaeoclimatology, Palaeoecology 438 (2015) 124–134

Contents lists available at ScienceDirect

Palaeogeography, Palaeoclimatology, Palaeoecology

journal homepage: www.elsevier.com/locate/palaeo

Late Holocene mangrove development and onset of sedimentation in the Yax Chen cave system (Ox Bel Ha) Yucatan, Mexico: Implications for using cave sediments as a sea-level indicator

S.V. Collins [a,*], E.G. Reinhardt [a], C.L. Werner [b], C. Le Maillot [c], F. Devos [c], D. Rissolo [d,e]

[a] School of Geography and Earth Sciences McMaster University Hamilton, Ontario L8P 4K1
[b] Science Director Woodville Karst Plain Project, United States
[c] Mexico Cave Exploration Project (MCEP), Centro Investigador del Sistema Acuifero de Quintana Roo A.C (CINDAQ), Global Underwater Explorers (GUE), Mexico
[d] Special Projects Coordinator Center of Interdisciplinary Science for Art, Architecture, and Archaeology (CISA3) Qualcomm Institute, UCSD Division of Calit2 University of California, San Diego, United States
[e] Research Associate Scripps Institution of Oceanography University of California, San Diego, United States

ARTICLE INFO

Article history:
Received 10 March 2015
Received in revised form 22 July 2015
Accepted 23 July 2015
Available online 7 August 2015

Keywords:
Cave sediments
Anchialine
Yucatan
Holocene
Hurricanes
Sea level
Mangrove

ABSTRACT

This study examines the relationship between the flooding of cenotes and formation of coastal mangrove with Holocene sea-level rise and the onset of aquatic sedimentation in Yax Chen, a cave system in Quintana Roo on Mexico's Yucatan Peninsula. Sediment depth measurements ($n = 180$) were collected along 2.7 km of an underwater cave passage and three cores were radiocarbon dated to examine both the extent and timing of sedimentation in the cave. Basal radiocarbon ages (~4 Ka) for aquatic sediments in the cave show that Holocene sea-level rise flooded cenotes, creating sunlit open water conditions with associated mangroves on the upper karst surface. These conditions initiated abundant and widespread sedimentation in the cave. Cenote surface area controlled the long-term sediment accumulation in the cave passages through primary productivity in the sunlit open water areas of the cenotes. This primary productivity was enhanced with mangrove formation, which causes funneling of precipitation and nutrient-rich waters into the cenotes from the mangroves. Accumulation histories from the radiocarbon-dated sediment cores ($n = 3$) were compared with accumulation histories in previously published studies including Actun Ha, Mexico and Green Bay Cave (GBC), Bermuda.

1. Introduction

Cave and sinkhole sediments have been used to document water level changes in anchialine systems and can be used as a proxy for sea level (Gabriel et al., 2009; van Hengstum et al., 2011, 2015). However, many of these studies were based on limited datasets or are speculative, as there are few studies which provide a basis for comparison. Recent research in Yax Chen (part of the Ox Bel Ha cave system) and the Outland Cave in Quintana Roo, Yucatan Peninsula, Mexico show that sedimentation can be ephemeral and non-continuous in cave passages (Collins et al., 2015a, 2015b). The study from the anchialine system of Sac Actun (Outland Cave) demonstrated the difficulty of reconstructing water levels and inferring sea level from cave systems with an upper karst terrain dominated by tropical forests (Collins et al., 2015a). The study emphasized that not only bottom elevation but more importantly ceiling elevation can control sedimentation in the cave. Research using sediment traps in Yax Chen showed the role of mangroves and cenote area on the sediment flux in downstream cave passages (3 years of data; Collins et al., 2015b). Little sediment was found in upstream cave passages dominated by tropical forest vegetation, while passages with overlying mangrove and large cenotes had abundant sediment. This study further examines long-term sedimentation patterns (1000s of years) in Yax Chen and the role of Holocene sea-level rise and mangrove formation which has important implications for using cave sediments as a sea-level indicator (van Hengstum et al., 2015).

1.1. The caves of Quintana Roo, Mexico

The Yucatan Peninsula is a carbonate platform of Paleogene to Quaternary age which has undergone multiple phases of diagenesis altering mineralogy and textural characteristics (Weidie, 1985). However, the platform has largely retained its sub-horizontal geometry with minimal differential tilting (Weidie, 1985; Coke, 1991; Beddows, 2004). The caves in the Yucatan have formed through repeated cycles of vadose and phreatic conditions associated with sea-level fluctuations over the Quaternary (Smart et al., 2006). The limestone matrix has a porosity of 17% but there is also a large anastomosing network of caves passages (>2 m dia.) with smaller hydrologic pathways through fractures and bedding planes (Beddows, 2004; Smart et al., 2006). Cave passage formation has been attributed to Mixing Zone (MZ) dissolution that occurs at the transition

* Corresponding author at: University of Toronto Mississauga, Department of Chemical & Physical Sciences Mississauga Ontario, L5L 1C6, Canada.
E-mail address: shawnvcollins@icloud.com (S.V. Collins).

http://dx.doi.org/10.1016/j.palaeo.2015.07.042
0031-0182/

between saline and meteoric groundwater which is undersaturated with respect to $CaCO_3$ – (Back et al., 1979, 1986; Hanshaw and Back, 1980; Beddows, 2004; Smart et al., 2006; Werner, 2007).

Cenotes form during sea-level low-stands when the weight of the ceiling exceeds the flexural strength of the limestone causing collapse resulting in a central breakdown deposit at the bottom of the cavern (Finch, 1965; Smart et al., 2006). The central breakdown deposit consists of angular, brecciated limestone boulders strewn on the floor of the cave. Cenotes (or sinkholes; karst windows) provide openings to the cave passages and act as point sources for allogenic sediments entering cave passage downstream (Pohlman et al., 1997; Gabriel et al., 2009; van Hengstum et al., 2010, 2015; Collins et al., 2015b). Organic matter (OM) and phytoplankton (e.g. diatoms) sediment enter the cave passages largely through this cenote point source as there is no primary productivity in the dark cave passages (Pohlman et al., 1997; Benavente et al., 2001; van Hengstum et al., 2010). Other allogenic sediments found in the cave system includes detrital carbonate (percolation from ceiling), transported speleothem fragments and minor clastic aeolian-derived dust (Schmitter-Soto et al., 2002; Lopez Fuerte et al., 2010; Collins et al., 2015a, 2015b). Autogenic sources of sediment are limited and include chemical precipitates such as calcite rafts, gypsum and chemoautotrophic microbial mats. Sediment can also enter through cracks and fissures in the bedrock but is minor in comparison to the cenotes (Mazda et al., 1990; Wolanski et al., 1992; Pohlman et al., 1997; Simon et al., 2007). Modern sediment trap studies in Yax Chen found a correlation between cenote area and mangrove extent with the amount of sediment entering the cave (Collins et al., 2015b).

1.2. Hydrogeology

The Yucatan has limited surficial water as the limestone has a high matrix porosity (~17%) with most of the water stored in the subsurface (>96%) and the cave passages accounting for ~99% of groundwater flow (Beddows, 2004). Due to this high porosity, water table elevation approximates sea level and there is minimal hydraulic gradient (10^{-5}), which equates to a water table rise of 1–10 cm/km (Beddows, 2004; Bauer-Gottwein et al., 2011; Milne and Peros, 2013; van Hengstum et al., 2015).

Groundwater in the Yucatan is density stratified with a meteoric lens (ML) on top of saline groundwater (marine water mass, MWM). Density contrasts between the warmer, denser MWM (~35 PSU) and the cooler ML (PSU < 1) are responsible for the stratification (Moore et al., 1992; Neuman and Rahbek, 2007). In Yax Chen, the MZ between the ML and MWM ranges from 10 and 14 mbsl and is stepped (~6–35 PSU; Collins et al., 2015b). The MZ can demonstrate changes in temperature, pH, dissolved oxygen and salinity depending on the location in the cave and the time of year (Esterson, 2003). There are numerous controls on the thickness and position of the MZ. Large-scale changes are a result of eustatic sea-level fluctuations. As sea level rises and falls, the aquifer tracks these changes and the MZ moves coincidently (Back et al., 1986; Raeisi and Mylroie, 1995; Florea et al., 2007). Short-term fluctuations in position and thickness of the MZ in the cave are a result of flow velocity changes, channel morphology and sinuosity of the cave passage (Smart et al., 2006; Beddows et al., 2007). The majority of mapped Yax Chen cave passages are within the ML (i.e. <10 mbsl).

Groundwater flow in Yucatan anchialine caves is low but varies with distance from the coastline with velocities ranging from 12 cm/s on the coast to ~1 cm/s 10 km inland (Moore et al., 1992). Cave passage morphology, flow patterns (Reynolds number) and sediment density can control patterns of sedimentation on the cave bottom (Beddows, 2004). The geometry of the passages are elliptical tubular, irregular and often subject to sudden elevational changes and abrupt bends (Smart et al., 2006). In addition to the changes in the shape, cave floors and ceilings tend to be obstructed with stalagmites, stalactites and central breakdown deposits, which can affect the rate and Reynolds

Fig. 1. The location of Cenote Yax Chen on the Yucatan Peninsula, Mexico.

number of the flow. These factors all increase the turbulent mixing in the cave and can affect localized sedimentation (Esterson, 2003; Beddows, 2004; Smart et al., 2006; Beddows et al., 2007). Broad depositional patterns are controlled by OM productivity in cenotes, which act as point sources for sediment entering the cave (Collins et al., 2015b).

1.3. Climate

Quintana Roo, Mexico has a tropical climate with heavy rains in the summer months and drier conditions in the winter (Metcalfe et al., 2000; Hodell et al., 2005). Seasonal variation is controlled by the movement of the intertropical convergence zone (ITCZ) with its northern movement bringing extensive precipitation from May to October, which overlaps with the hurricane season in the Caribbean (June to November; Hanstenrath and Greischar, 1993; Hughen et al., 1996; Peterson et al., 1991). On average, the Yucatan Peninsula receives 550–1500 mm of precipitation per annum (Bauer-Gottwein et al., 2011). During the dry season (November to April) the ITCZ moves south resulting in dry, cool conditions (Peterson et al., 1991; Hanstenrath and Greischar, 1993; Hughen et al., 1996). The average temperature for the area ranges from 34 °C in the summer months to 25 °C in the winter (Beddows, 2004; Hodell et al., 2005; Bauer-Gottwein et al., 2011).

1.4. Study site

Yax Chen is part of the Ox Bel Ha cave system, which is 9 km south of the town of Tulum and on the northern border of the Sian Ka'an Biosphere (Figs. 1, 2a). The Ox Bel Ha cave system is currently one of the world's longest underwater caves with over 242 km of explored underwater passage (Quintana Roo Speleological Survey, 2014). Yax Chen is a 2.7-km-long section of Ox Bel Ha that trends in a NW direction inland from the coastline with access to the cave

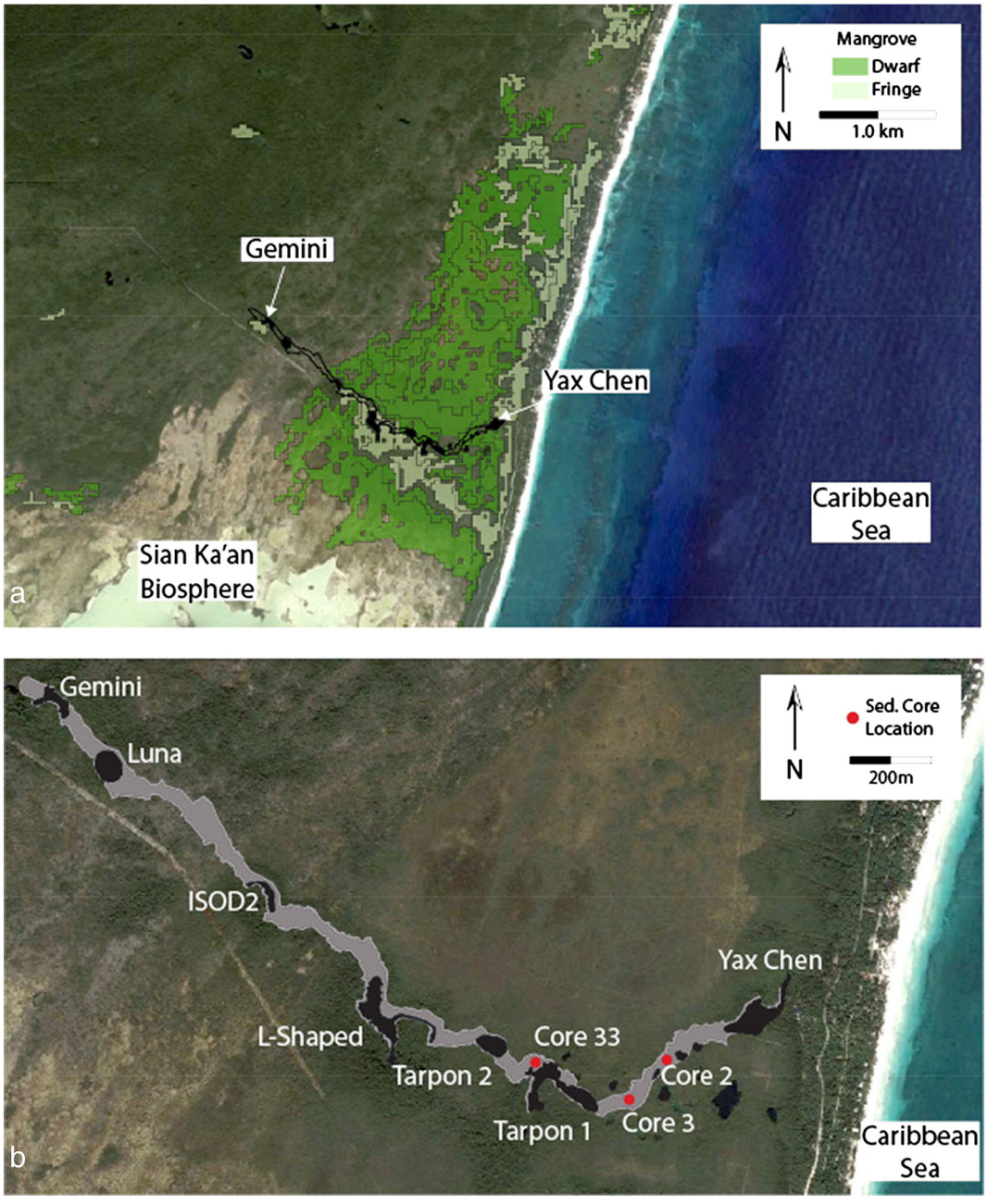

Fig. 2. (a) Partial results of Landsat 5 supervised classification of mangrove forest in the Tulum Region (modified after Meacham, 2012). (b) Location of mapped cenotes and core locations in Yax Chen, Quintana Roo, Mexico.

through a large cenote (Cenote Yax Chen) proximal to the coast (Fig. 2b). Downstream from Cenote Yax Chen porous matrix and fractures through the beachhead connect to the open ocean. Yax Chen has seven large cenotes which range in size from 1600 to 9000 m^2 and at least five other unnamed smaller cenotes (250–1050 m^2; Fig. 2b). The average depth of the mapped sections of the cave are ~10 mbsl but some sections are >14 mbsl. The explored cave passages are generally subperpendicular to the coast with some passages trending sub-parallel, with an average width of 25 m. The flow direction is generally from west to east moving towards the Caribbean coast.

Collins et al. (2015b) conducted a sediment trap study of Yax Chen over three years (May 2011–May 2014) capturing the effects of Hurricane Ingrid (September 2013) and showed how cenote size and mangrove coverage influenced sedimentation in downstream cave passages. The present study examines whether these trends apply to long-term sedimentation patterns in Yax Chen over the mid-late Holocene.

2. Methods

2.1. Cave mapping

The cave from cenotes Gemini to Yax Chen were mapped using the exploration line that generally followed the central area of the passage. The orientation of the passage was mapped using compass bearings and distance between tie-off points on the exploration line. Sidewall measurements from the exploration line (~every 30 m) were recorded using a tape measure to obtain passage widths while bottom and ceiling heights were collected using a digital depth gauge (±0.1 m) to obtain the overall geometry of the passage. Field measurements were compiled in ArcGIS (Esri Geographical Information System v10.2) and spatially corrected with cenote GPS locations (Garmin etrex) and overlain on pansharpened Landsat 7 satellite imagery (15 m resolution) provided by Google Earth™.

The area of each mapped cenote in Yax Chen was calculated remotely using satellite imagery available on Google Earth™. The satellite image was imported into ArcGIS and georectified to insure accurate positioning with existing cave survey maps. Each cenote was digitized into polygons and the area for each polygon was calculated.

2.2. Sediment depth

A total of 180 sediment depth measurements were collected by self-contained underwater breathing apparatus (SCUBA) throughout the length of Yax Chen using foldable avalanche poles (3 m), which were graduated every centimeter. This provided an average elevation of the cave bottom that may have included underlying speleothems and cave breakdown. Depth of the sediment water interface and ceiling height for each location was measured using a digital depth gauge (±0.1 m). At least three measurements at each station were recorded across the width of the cave passage to provide an average accumulation thickness (Fig. 5). The sediment depth data was tabulated and entered into ArcGIS to calculate the kriging weights and plot the final models. Assessment of the data revealed that the sediment depth data consisted of a moderate number of points, was slightly non-stationary and non-parametric. Based on these factors, ordinary kriging was determined to be the most appropriate interpolation method for this dataset. Data was plotted and a model fitted to the semivariogram to determine coefficients and values at unmeasured locations to determine the error of the estimate. The validity of the model was tested using cross-validation, which compared the measured sediment depths with modeled values in the interpolation and calculated statistics on the difference (Arlot and Celisse, 2010).

2.3. Sedimentation rate

Sediment cores (5 cm diam.) were collected using SCUBA at depths of 9.2 (Core 2 and Core 33) and 7.6 mbsl (Core 3). Cores were logged and bulk OM used for radiocarbon dating (AMS) as there were no seeds or discernible OM that could be isolated. Samples were analyzed at Beta Analytic, Miami, Florida, NOSAMS, Woods Hole Oceanographic Institution, Massachusetts and Direct AMS, Seattle, Washington. Raw radiocarbon

Table 1
Conventional and calibrated radiocarbon ages measured by atomic mass spectrometry, from Gabriel and Reinhardt (2006); van Hengstum et al. (2010) and van Hengstum et al. (2011).

Location	Core No.	Sample Depth (mbsl)	Depth (cm)	Laboratory no.	Age ^{14}C yr B.P.	Age Range (2σ) cal yr B.P.
Aktun Ha	C2	−16.07	7	Beta-279531	570 ± 40	581–651
	C2	−16.10	10	Beta-239981	780 ± 40	666–766
	C2	−16.12	12	Beta-271308	750 ± 40	653–739
	C2	−16.16	16	Beta-272082	800 ± 40	673–782
	C2	−16.21	21	Beta-239982	2640 ± 40	2722–2811
	C2	−16.26	26	Beta-279532	2480 ± 40	2434–2718
	C2	−16.31	31	Beta-271309	3110 ± 40	3239–3404
	C2	−16.36	39	Beta-239983	3210 ± 40	3361–3486
Ox Bel Ha	C2	−9.29	9	Beta-257280	950 ± 40	776 -934
	C2	−9.49	29	Beta-257281	1840 ± 40	1696–1874
	C2	−9.71	51	Beta-257282	2460 ± 40	2362–2618
	C2	−9.93	73	OS-74418	3310 ± 30	3466–3618
	C3	−7.81	21	OS-74462	435 ± 35	439–533
	C3	−8.01	41	OS-74420	1410 ± 30	1286–1358
	C3	−8.21	61	OS-74422	2270 ± 25	2301–2346, 2178–2243
	C3	−8.29	69	OS-74423	2730 ± 25	2769–2868
	C3	−8.39	79	OS-74424	3240 ± 30	3388–3491
	C33	−9.25	5	D-AMS 008975	Modern	Modern
	C33	−9.38	18	D-AMS 008367	725 ± 26	652–699
	C33	−9.64	44	D-AMS 008366	953 ± 26	796–885
	C33	−9.79	59	D-AMS 008368	1339 ± 27	1239–1303
	C33	−9.95	75	D-AMS 008369	1724 ± 28	1564–1701
Green Bay Cave Bermuda	GBC5	−19.65	15	OS-79473	645 ± 25	246–378
	GBC5	−19.78	28	OS-78020	1610 ± 25	1096–1253
	GBC5	−19.81	31	OS-78019	2040 ± 25	1533–1687
	GBC5	−19.88	38	OS-78451	3590 ± 30	3834–3974
	GBC5	−19.96	46	OS-74180	3800 ± 40	4082–4298
	GBC5	−20.00	50	OS-74179	4930 ± 45	5590–5742
	GBC5	−20.02	52	OS-80321	6800 ± 50	7233–7418
	GBC5	−20.11	61	OS-79218	7160 ± 65	7509–7765
	GBC5	−20.15	65	OS-79474	11100 ± 65	12802–13086

ages were calibrated with the northern hemisphere terrestrial calibration curve IntCal13 (Reimer et al., 2013) using the R statistical software package Clam (Blaauw, 2010; version 2.2, Table 1). Sediment accumulation histories used an inferred date of 0 years BP (±1 years BP) for the core top and a linear age model to fit the data.

Collins et al. (2015b) used sediment trap data to calculate modern sedimentation rates for Yax Chen and found the average bulk density of the sediment was 0.01 g/cm^3. Sedimentation rates for the cores were calculated using this average bulk density estimate. Based on the volume of the 5 cm core tube, sedimentation rate was calculated using the following formula:

$$Sedimentation\ Rate = \left\{\frac{BD * VCT * L}{Y * 365}\right\}$$

BD = bulk density of mangrove gyttja
VCT = volume of core tube (cm)
L = length of core tube (cm)
Y = number of years

Sedimentation rate was calculated for radiocarbon-dated intervals in the cores, and compared with modern day rates reported in Collins et al. (2015b).

2.4. Mangrove distribution

Meacham (2012) used the physiognomic classification of mangrove forests developed in Lugo and Snedaker (1974) to map the extent of mangroves in the vicinity of Yax Chen. The classification used the spectral signature of mangrove leaves and other vegetation to discriminate fringe and dwarf classes of mangrove forest. Fringe mangroves tend to dominate in areas of protected shorelines where the elevations are higher than mean high tides. Fringe mangroves tend to have well-developed prop roots that are excellent at entrapping sediment (Lugo and Snedaker, 1974). Dwarf mangroves are generally found in flat coastal areas. The most characteristic feature of the dwarf mangrove stand is the limited vertical extent of the trees <1.5 m (Lugo and Snedaker, 1974). The physiognomic classification system is not species-specific, however; Mexico has only three species of mangrove including *Rhizophora mangle* (red mangrove), *Avicennia germinans* (black mangrove) and *Laguncularia racemosa* (white mangrove; Lopez Fuerte et al., 2010).

3. Results

3.1. Age model and sedimentation rates

All three cores from Yax Chen contained fine OM (gyttja) with only minor variation in color due to variable amounts of small shell fragments. Both Cores 2 and 3 penetrated to the cave bottom (limestone) while Core 33 did not reach refusal (Fig. 2b).

The age model for Core 2 used four radiocarbon dates, contained no age reversals and had a 95% confidence interval ranging from 131 to 355 years (mean = 198 years; Fig. 3; Table 1). The age model for Core 3 used five dates and had a 95% confidence interval ranging from 70 to 369 years (mean = 152 years; Fig. 3; Table 1). The age model for Core 33 used four dates and had a 95% confidence interval ranging from 4 to 147 years (mean = 79 years; Fig. 3; Table 1; the sample at 5 cm provided a modern radiocarbon age). For comparison, an age model was calculated from the nearby Actun Ha cave system using

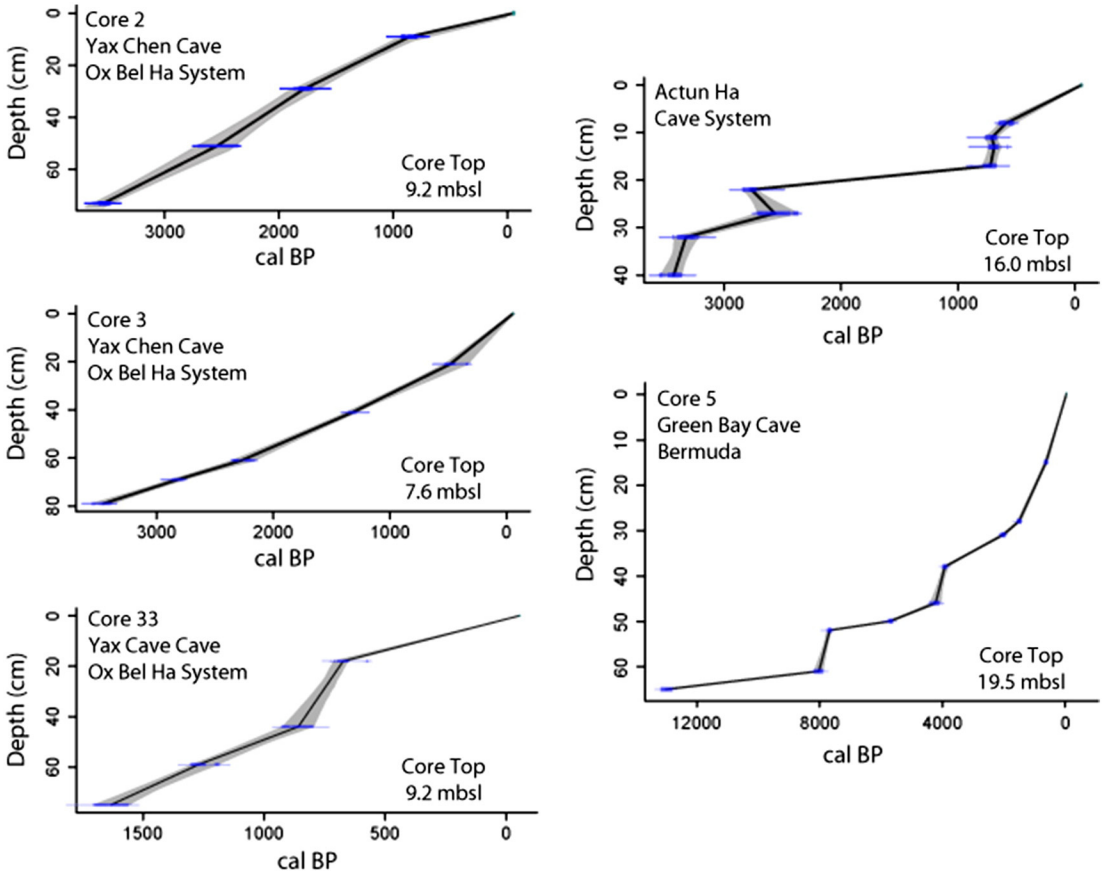

Fig. 3. Age/depth models calculated using Clam R statistical software for sediment cores from Yax Chen, Actun Ha (van Hengstum et al., 2010) and Green Bay Cave, Bermuda (van Hengstum et al., 2011). Blue lines represent calibrated distributions of dated material. Black lines represent the age-weighted mean value for a given depth. The grey shaded area corresponds to the 95% confidence interval for the age/depth model. Note: Core 33 did not reach refusal.

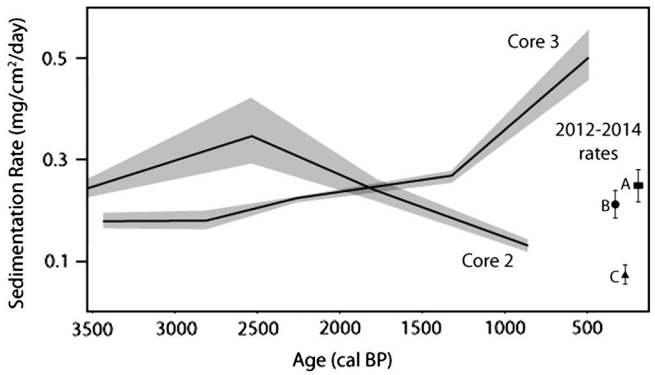

Fig. 4. Calculated sedimentation rates for Cores 2 and 3 from Yax Chen. Also plotted are modern sedimentation rates and standard deviations from Collins et al. (2015b). Point A is the modern sediment flux downstream of the mangrove forest. Point B is the modern overall sediment flux for the entire Yax Chen Passage. Point C is the modern sediment flux upstream of the main mass of mangrove forest (see Fig. 5 for detailed mangrove extent).

the radiocarbon dates from van Hengstum et al. (2010; Core 2) and two additional radiocarbon dates (Table 1). The core was retrieved 40 m downstream of Cenote Carwash at a depth of 16 mbsl (see Fig. 8 for location). The resulting age model using eight radiocarbon dates had a 95% confidence interval ranging from 4 to 338 years (mean = 127; Fig. 3; Table 1) and had two age reversals that were within the uncertainty of the model. Core 5 from GBC, Bermuda was also age-modeled based on the radiocarbon ages in van Hengstum et al. (2011). The age model for GBC core 5 used nine radiocarbon dates, contained no age reversals and had a 95% confidence interval ranging from 4 to 391 years (mean = 145 years; Fig. 3; Table 1).

Based on the age models, accumulation histories in Yax Chen were very similar and largely linear compared to GBC and Actun Ha. Cores 2 and 3 have similar basal ages (~3500 cal yr BP) and accumulation profiles, while Core 33 showed a largely linear accumulation rate but had a basal age of only ~1600 cal yr BP, as the core did not reach refusal. The upper age (~700 cal yr BP, 18 cm) may be an outlier as a result of contamination with older OM fragments, as radiocarbon dating of material at 5 cm (not included in the age model) was determined to be modern (Table 1) and better fits the relationship with the lower 3 ages. The accumulation rate of sediment in Core 33 is ~ 2× the rate in Cores 2 and 3.

In contrast, the cores from Actun Ha and GBC show stepped sediment accumulation histories that indicate episodic deposition of sediment with hiatuses or possibly erosional events between depositional episodes (Fig. 3). The basal age of Actun Ha is similar to the Yax Chen cores (~3500 cal yr BP) while the GBC is much older (13,000 cal yr BP) likely due to its increased depth.

Sedimentation rates calculated using bulk density values from (Collins et al., 2015b) showed slight changes through time varying from ~0.1 to 0.5 ± 0.05 mg/cm^2/day (Fig. 4). The mean accumulation rate for the two cores was 0.3 ± 0.05 (1σ) mg/cm^2/day, which was comparable to the average accumulation rates calculated for the modern sediment traps (Point B in Fig. 4; Collins et al., 2015b). Points A and C represent the mean sedimentation rate downstream and upstream of the mangrove extent, respectively.

3.2. Sediment depth, kriged surface

Sediment depth measurements were taken at over 60 stations with each station consisting of three measurements transecting the width of the cave passage. The ceiling heights and average sediment thickness ($n = 3$) were plotted along the length of Yax Chen showing the relationship with the overlying mangrove (Fig. 5). The average sediment thickness for the entire cave was 1.21 ± 0.75 (1σ) m with a maximum thickness of 3.6 m. Sediment thickness was lowest in the western section of the passage (mean = 1.03 m) dominated by overlying tropical forest vegetation and increased (mean = 1.27 m) moving east with the presence of mangrove (Fig. 5).

The kriged interpolated sediment depth surface was overlaid on the extent of the mangrove to show the spatial relationships (Fig. 6). Cross-validation of the model results indicated that the average error for sediment depth was between 0.18 and 0.53 m, with the largest error in the cenotes. This was expected as minimal measurements were taken in the cenotes as there was little exposed sediment. As previously mentioned, collapsed central breakdown deposits in the cenotes and also in the cave preferentially concentrated sediment in the voids and crevices between boulders. The model indicated the sediment thickness was deeper east

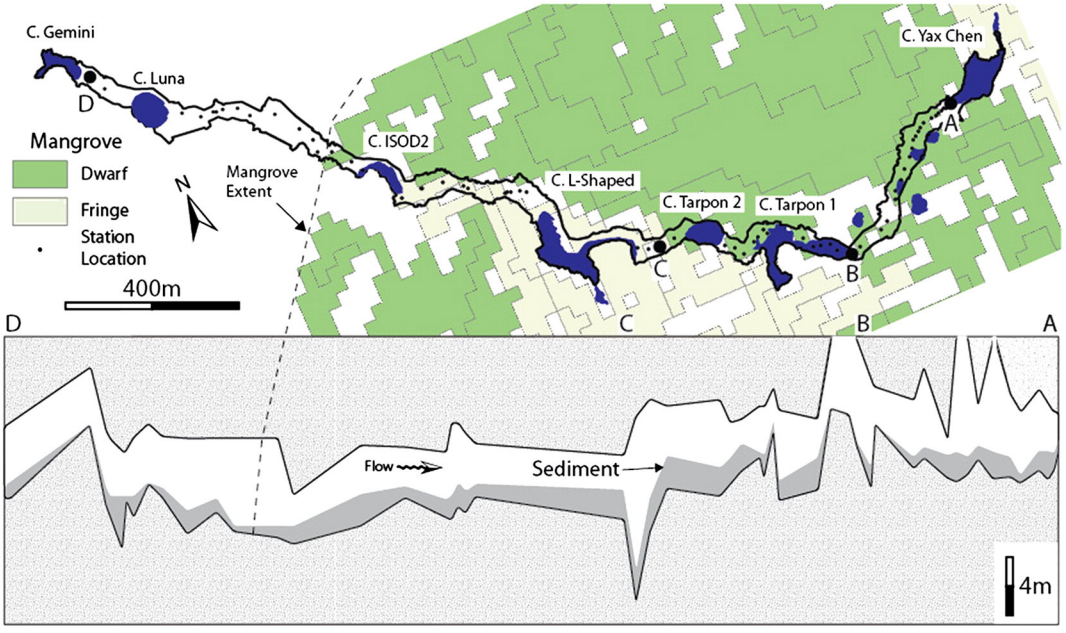

Fig. 5. Average sediment depth profile in the eastern section of the Ox Bel Ha cave system from Cenote Yax Chen to Cenote Gemini (based on three measurements at each station). The vector map of the extent of overlying fringe and dwarf mangrove is shown for comparison (vertical exaggeration = 100; vector overlay, modified after Meacham, 2012).

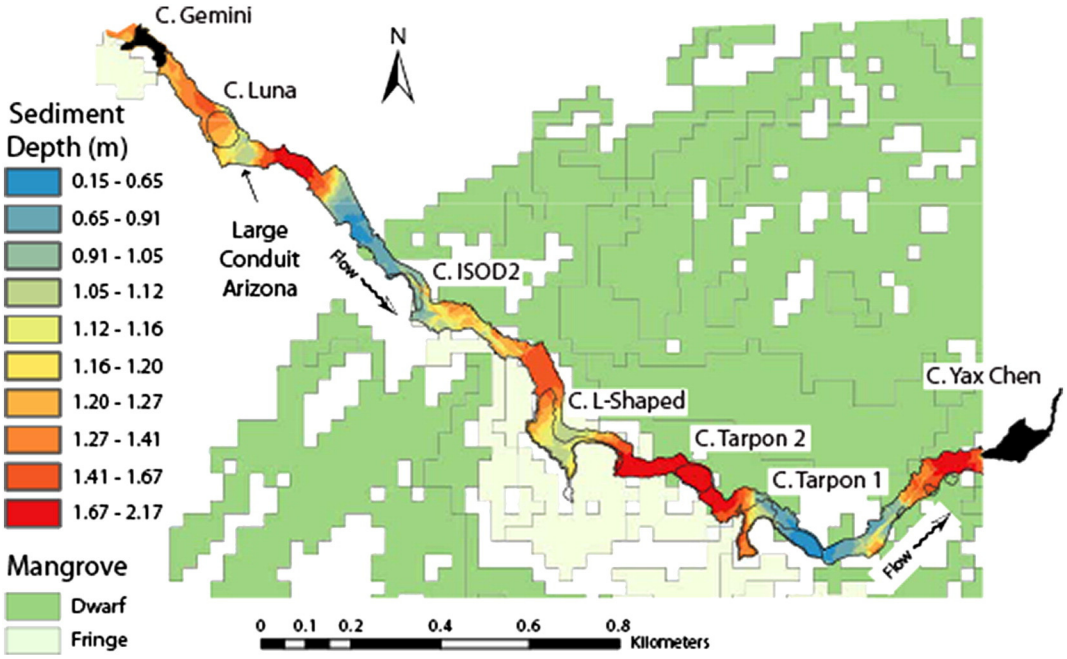

Fig. 6. Interpolated sediment depth surface for Yax Chen showing areas of increased sediment thickness. Partial results of supervised mangrove classification, overlaid to show relationship between sediment thickness and mangrove forest (modified after Meacham, 2012).

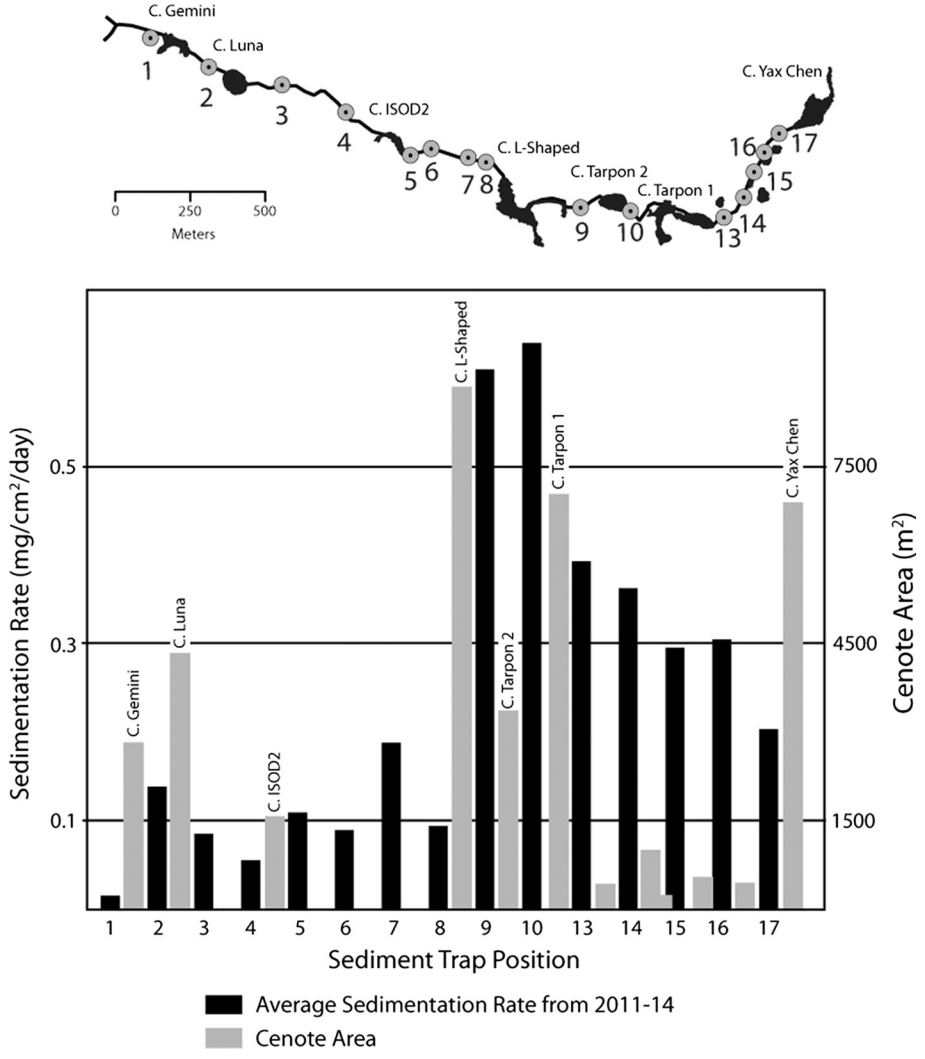

Fig. 7. Average sedimentation rate calculated in mg/cm^2/day from 2011 to 2014 and cenote area in m^2, plotted in order from Cenote Gemini to Cenote Yax Chen (Collins et al, 2015b).

of the mangrove with the greatest concentration of sediment located between Cenotes L-Shaped and Tarpon 2 (1.67–2.17 m) where there is fringing mangrove (Fig. 6). The interpolation also identified two zones in the area with overlying tropical forest vegetation, which had elevated sediment thicknesses above the mean of 1.03 m. The model predicted the sediment thicknesses in these regions as 1.67–2.17 m (red) and 1.16–2.17 m (yellow), highlighting localized zones of increased sediment thickness not readily apparent on Fig. 5.

3.3. Cenote area and modern sedimentation rates

The area of each cenote was plotted against the average sedimentation rate for 2011–2014 reported in Collins et al. (2015b; Fig. 7). The cenotes ranges in size from 250 to 9000 ± 30 m^2 with the mean size being 3200 ± 30 m^2. L-Shaped Cenote was the largest with an area in excess of 9000 ± 30 m^2 (Figs. 2b, 7). The data showed that currently, the average sedimentation rate upstream of L-Shaped Cenote is 0.09 ± 0.02 mg/cm^2/day, while in downstream locations it is four times greater (0.4 ± 0.07 mg/cm^2/day). Sedimentation rates increase downstream of L-Shaped Cenote with contributions of sediment from cenotes Tarpon 1 and 2 and other smaller cenotes.

4. Discussion

4.1. Mangrove development and the onset of cave sedimentation in Yax Chen

Rising Holocene sea level flooded the Yax Chen cave passages (~10 mbsl) at ~ 7500 cal yr BP based on the Toscano and Macintyre (2003) and Milne and Peros (2013) sea-level curves (Fig. 8). However, the basal ^{14}C age from the aquatic sediments in Core 2 and Core 3 is ~ 3500 cal yr BP, indicating Holocene sedimentation in the cave did not begin until ~4000 years after flooding of the cave bottom. During cave flooding (~7500 cal yr BP) until the cave passages were completely flooded (~4000 cal yr BP) sedimentation in the cave was likely low and consisted predominately of calcite rafts and minimal fine OM (Collins et al., 2015a, 2015b; Fig. 9). The ages for the onset of sedimentation in Yax Chen are better explained with the rise of sea-level flooding cenotes producing sunlit open water conditions for primary productivity but also flooding the subaerial karst terrain and mangrove formation which, based on the sea level curves, occurred at ~4500–3800 cal yr BP (Toscano and Macintyre, 2003; Milne and Peros, 2013; Fig. 8). As water level rose within the cenotes and overtopped the breakdown piles, connection between the cave passages and cenotes would allow downstream transport of particulate OM (Gabriel et al., 2009). Our basal ages from Yax Chen also match this flooding age and the onset of mangrove development recorded at other locations along the coast (Torrescano and Islebe, 2006; Fig. 8). Torrescano and Islebe (2006) documented the initiation of mangrove at El Palmar swamp located southwest of Cenote Yax Chen, near the City of Chetumal by ~3800 cal yr BP (see Fig. 1 for location; Table 2). Basal mangrove peats ^{13}C dated at Casa Cenote show a similar age (3395–3788 cal yr BP) and are coincident with the basal ages from Yax Chen (Fig. 8; Table 2). During this period, sedimentation in the cave was high, consisting of OM derived from upstream cenotes (Fig. 9).

Based on the modern sediment trap study from Collins et al. (2015b), it appears, but is still supposition, that mangrove peat creates an aquitard slowing downward percolation of rainwater through the vadose zone. In mangrove areas, precipitation funnels nutrient-rich waters into the cenotes during the seasonal drop in the water table during the dry season (November–April). This nutrient-rich water then causes increased primary productivity in the sunlit cenotes and the draining water also causes slightly increased flows into the downstream cave passages (Moore, 1999). In the sediment trap study, there was a strong direct relationship between cenote area and sediment flux with the presence of the mangrove (Collins et al., 2015b; Fig. 7). In contrast,

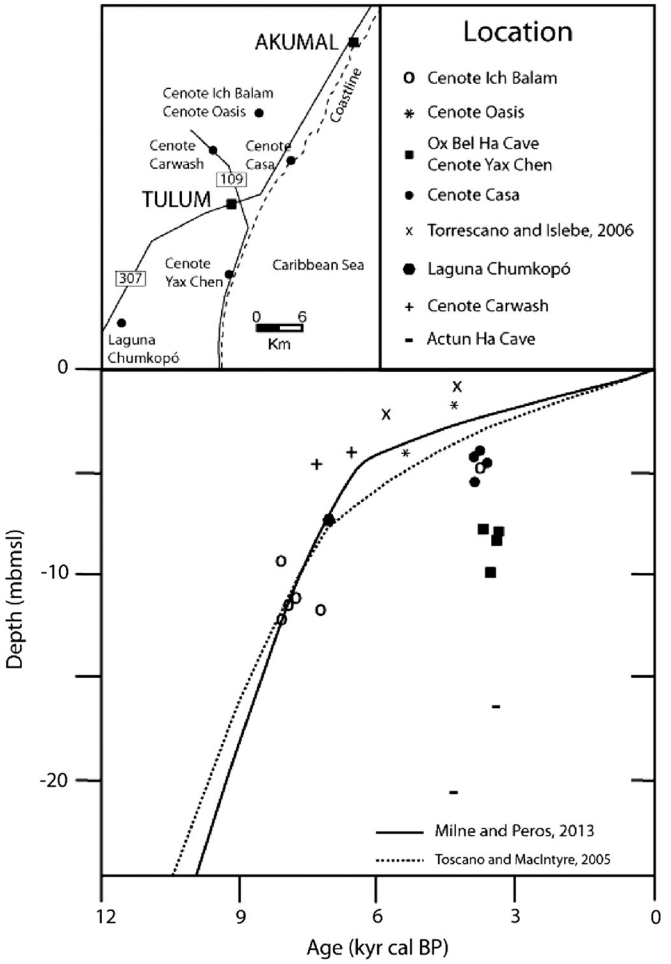

Fig. 8. Radiocarbon ages from previous studies at eight different locations around Quintana Roo, Mexico were plotted on the local Caribbean sea-level curve from Toscano and Macintyre (2003) and Milne and Peros (2013). Dating results: Cenotes Ich Balam and Oasis from Collins et al. (2015a); Ox Bel Ha Cave/Cenote Yax Chen from Gabriel and Reinhardt (2006), unpublished; Cenote Casa from Kovacs and Gregory (2013), unpublished; El Palmar Swamp from Torrescano and Islebe (2006); Laguna Chumkopó from Brown et al. (2014); Cenote Carwash from Gabriel et al. (2009); Actun Ha from van Hengstum et al. (2010).

tropical forest terrains, with their thin soils, allow rainwater to immediately penetrate through the vadose zone to the water table resulting in minimal nutrient inputs to cave passages (Pohlman et al., 1997).

This effect is also seen in the long-term sediment depth data where areas upstream of L-Shaped Cenote generally have thinner sediment deposits vs. downstream areas where they are thicker (Figs. 5, 6). This corresponds with both more extensive mangrove but also increased cenote area and associated primary productivity, which matches similar trends in the modern sediment trap study (Collins et al., 2015b). There are departures from this trend, notably downstream from Cenote Luna where the kriged data shows higher sediment depths, which may be due to inputs from side cave passages that connect to the Sian Ka'an Biosphere wetlands. Cenote Luna has a relatively large surface area and nutrient inputs from side passages may be increasing primary productivity and sedimentation in the downstream areas of Yax Chen. Sediment coverage thins to negligible amounts upstream of Cenote Gemini (Figs. 5, 6). As sea-level rise continues, sedimentation would be expected to extend further inland as new mangrove stands develop on the karst surface (McKee et al., 2007).

Similar but multiple phases of shifts in sedimentation are likely causing stepwise sediment accumulation patterns in cores from

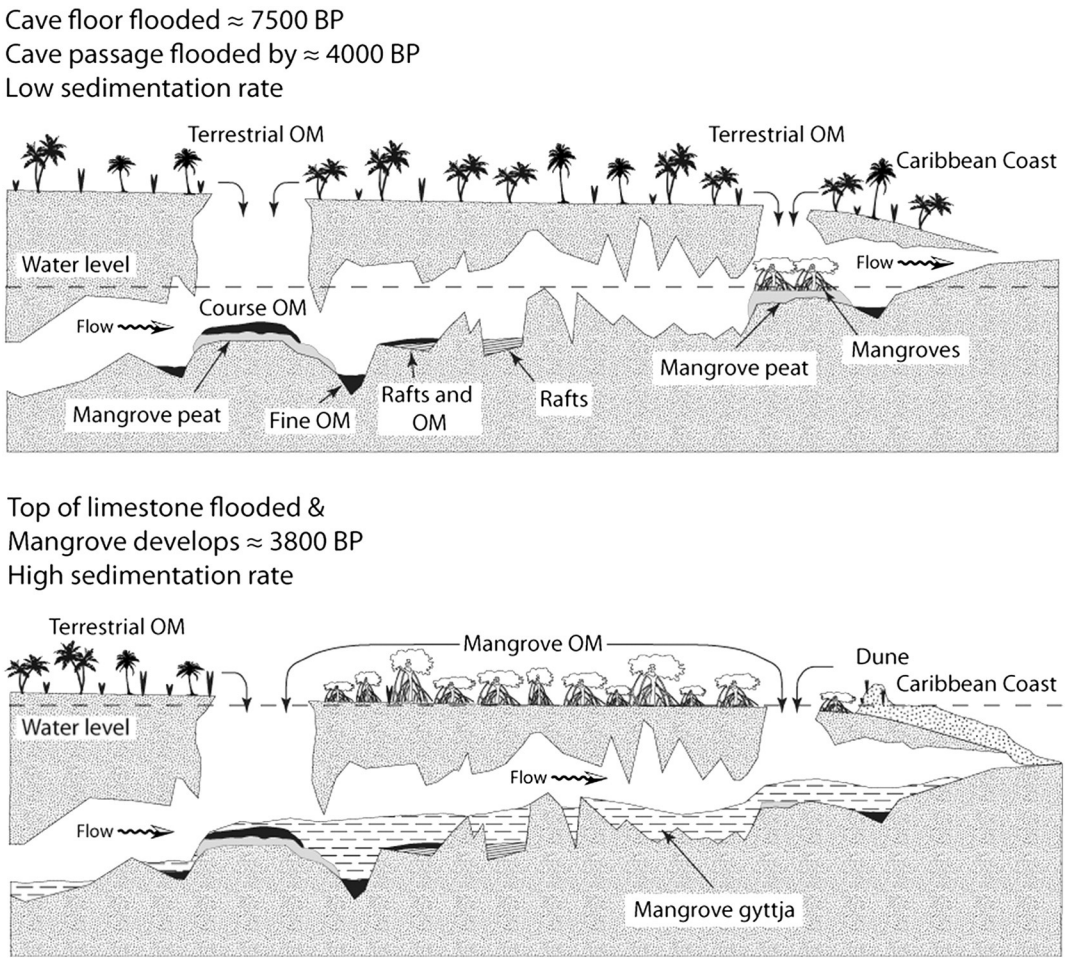

Fig. 9. An interpretative drawing of the initiation of sedimentation for Yax Chen Cave and the nature of sediment being deposited. Initial inundation of cave passage with rising sea level results in low sedimentation rates limited to cenote proximal zones of the cave. Initiation of mangrove swamp over Yax Chen Cave resulted in elevated sedimentation in the cave passage. Cave flooding did not correspond directly with initiation of sedimentation in the cave passage.

Table 2
Conventional and calibrated radiocarbon basal sediment ages measured by atomic mass spectrometry from various locations around Quintana Roo, Mexico.

Location (Author)	Core/Sample No.	Sample Depth (mbsl)	Depth (cm)	Laboratory no.	Age ^{14}C yr B.P.	Age Range (2σ) cal yr B.P.
Cenote Ich Balam	C6	−4.9	26	D-AMS 002372	3510 ± 31	3698–3865
(Collins et al., 2015a)	C2	−9.4	131	Beta 333187	7270 ± 40	8009–8172
	C3	−11.2	38	D-AMS 002368	6994 ± 31	7742–7817
	C1	−11.5	64	D-AMS 002363	7088 ± 31	7914–7970
	C5	−11.8	120	Beta 333188	6300 ± 40	7163–7310
	C4	−12.3	77	D-AMS 002374	7269 ± 38	8010–8170
Cenote Oasis	OAC3	−1.8	76	D-AMS 003400	3887 ± 38	4230–4420
(Collins et al., 2015a)	OAC2	−4.1	66	D-AMS 003397	4704 ± 29	5322–5418
Ox Bel Ha Cave/Cenote Yax Chen	C1	−7.8	32	Beta-244014	3460 ± 40	3636–3836
(Gabriel and Reinhardt, 2006)	C4	−7.9	43	OS-74426	3160 ± 30	3343–3447
	C3	−8.4	80	OS-74424	3240 ± 30	3388–3491
	C2	−10.0	75	OS-74418	3310 ± 30	3466–3618
Cenote Casa	1	−4.0	-	D-AMS 002350	3519 ± 31	3701–3874
(Kovacs and Gregory, 2013)	2	−4.3	-	D-AMS 002353	3607 ± 39	3831–3994
	4	−4.6	-	D-AMS 002357	3392 ± 29	3567–3699
	3	−5.5	-	D-AMS 002355	3579 ± 33	3826–3977
El Palmar Swamp	C1	−0.8	80	NSRL 11098	3870 ± 50	4153–4418
(Torrescano and Islebe, 2006)	C1	−2.2	220	NSRL 11099	5080 ± 40	5739–5913
Laguna Chumkopó	CK2	−7.3	91	Beta-270693	6160 ± 40	6951–7164
(Brown et al., 2014)						
Cenote Carwash	C1	−4.1	6	Beta-226967	5790 ± 40	6488–6675
(Gabriel et al., 2009)	C1	−4.6	57	Beta-235036	6390 ± 40	7262–7418
Actun Ha Cave	C2	−16.4	40	Beta-239983	3210 ± 40	3361–3486
(Van Hengstum et al., 2010)	C4	−20.5	53	Beta-237363	3890 ± 40	4229–4422

GBC, Bermuda and Actun Ha, Mexico (Fig. 3). In GBC, the shift in xsedimentation occurs with the abrupt onset of carbonate mud deposition throughout the cave (C12, C7, C11, C2; Fig. 8 in van Hengstum et al., 2011). When sea level breaches a sill at the entrance of GBC connecting Harrington Sound (a marine embayment) with the cave passages, micrite from the lagoon is transported into the cave. In Actun Ha, the basal age for the onset of cave sedimentation is too young (~3400 cal yr BP) for its elevation (−16.4 mbsl) but similar in age to Yax Chen. The coincident age is likely due the topography of Cenote Carwash (entrance to Actun Ha), which is shallow (−4.5 mbsl). Sea-level rise and flooding of the central breakdown deposit occurred after (~6500 cal yr BP) and continued to rise thereafter forming deeper, open water conditions in the cenote (Gabriel et al., 2009). The initiation of sedimentation likely represents the transition to open water conditions in the cenote with its associated primary productivity but also, connection of the two sections of the cave (upstream and downstream) allowing movement of sediment from the sunlit cenote into the cave passage through increased flow. This occurred at approximately the same time as the formation of the mangrove around Yax Chen with rising Holocene sea level.

The emphasis of this study is how inherited topography (i.e. karst surface) and sea-level change can dictate the distribution and development of surficial vegetation; additionally, however, the hydrological connection and flow regime in the cave passages are important variables on cave sedimentation. This in turn determines when, and what type of sediment will be deposited in the cave, which will be affected by climate-induced hydrological change (e.g. more rainfall events) but it does appear that sea levels trigger abrupt shifts in sedimentation in the cave (van Hengstum et al., 2011, 2015). The nature of the phase-shift in sedimentation will depend on cave physiography and its connection with outside sources of sediment; however, it is sea level coupled with the topography that is triggering large and rapid shifts in sedimentation.

4.2. Implications for using cave sediments as a sea level indicator

Plots of basal peats/aquatic sedimentation from a variety of locations in the vicinity of Yax Chen show discrepancies from Caribbean sea-level curves (Fig. 8). Some points show good correlation, while others demonstrate considerable departures (~16 m). Generally, the sites that were located in cenotes had good correspondence (e.g. Chumkopó, Carwash), while cave sediments tended to show some significant discrepancies. Yax Chen and Actun Ha have notable departures as discussed; however, data from Cenotes Ich Balam and Oasis with ages that are too old for a given depth likely reflect contamination with older allochthonous OM. Cenotes have better correspondence between the onset of sedimentation and flooding likely because OM has a higher chance of accumulating and being preserved in the open water areas. Deposition in the cenote is a result of gravitational settling and does not rely on transportation processes necessary for deposition in the cave (see also, Collins et al., 2015a; Fig. 9). As discussed in Gabriel et al. (2009), it isn't until the water table reaches the top of the central breakdown deposit that mangrove and other vegetation can grow, allowing autochthonous sedimentation in and around the open waters zones of the cenote. In the case of Cenotes Ich Balam and Oasis in the Outland cave system, basal ages demonstrated a better fit with sea level. This was shown to be the result of bats transporting OM (seeds and guano) deep into the cave, which was then preserved in shallow water on the cave bottom allowing for better resolution of sea-level changes. In the Actun Ha system, this is not the case, even though distances from the cenote are very similar. As discussed in Collins et al. (2015a), numerous cores are required to isolate the flooding age for cave passages. Basal ages in these circumstances should be considered as a minimum date for cave inundation, as flooding may have occurred previous to sediment deposition/preservation. The basal ages likely reflect a change in the hydrology as explained, causing movement of sediment into the cave with water level rising and flooding the central breakdown deposit. The ceiling height and its relationship with flooding is also very important for the movement of floating OM but also airway access for bats and birds entering the cave (Collins et al., 2015a). Work at the Hoyo Negro archaeological site demonstrated how these airways affected the loci of OM deposition in the cave with rising sea level over the Holocene (Collins et al., 2015a), and emphasized the need to measure and document the cave physiography (bottom and ceiling heights) to understand what controls sedimentation in the cave. As demonstrated in Hoyo Negro but also GBC, Bermuda, the elevation of sills or restrictions (e.g. ceiling) is required information to associate sediment records with sea-level change in the cave environment.

5. Conclusions

Abundant OM sediment began accumulating and being preserved in Yax Chen at ~3500 cal yr BP when the upper karst terrain became flooded with Holocene sea-level rise, allowing increased primary productivity in open water cenotes, increased hydraulic connectivity between cave passages and the development of mangroves. These results match the ages for the establishment of mangroves from nearby sites (e.g. 3800 cal yrs BP; Chetumal; Torrescano and Islebe, 2006) on the coast. The development of mangroves, coupled with cenote size, largely determined the long-term pattern of sedimentation in the cave as measured with sediment thickness. This trend matched those from modern sediment trap studies conducted previously in Yax Chen (Collins et al., 2015b). Based on these results, basal ages for the onset of aquatic cave sedimentation should be scrutinized with respect to karst physiography and their connectivity with surficial terrestrial environments as phase shifts in sedimentation may not be coincident with the flooding of the cave bottom with sea-level rise.

Acknowledgements

The authors would like to thank Dr. Todd Kincaid and one anonymous reviewer for their insightful reviews and comments on the original manuscript. We would also like to thank David Carrillo for his cartography skills and AutoCAD digitation of Yax Chen Cave Map. We gratefully acknowledge the support of Global Underwater Explorers, The Mexican Cave Exploration Project, Cindaq, and the staff at Zero Gravity for dive support and logistics. This research was possible with the MCEP Science Week volunteers from around the world (especially the Dutch contingent). Special thanks go to Onno van Eijk, Ali Perkins, Arno Mol, Jan Duikt, Steve and Chantel Blanchard for repeated support each year. Funding was provided by National Sciences and Engineering Research Council of Canada (EGR-Discovery); National Geographic Research and Exploration Grant (EGR).

References

Arlot, S., Celisse, A., 2010. A survey of cross-validation procedures for model selection. Stat. Surv. 4, 40–79.

Back, W., Hanshaw, B.B., Pyle, T.E., Plummer, L.N., Weidie, A.E., 1979. Geo-chemical significance of groundwater discharge and carbonate dissolution to the formation of Caleta Xel Ha, Quintana Roo, Mexico. Water Resour. Res. 15, 1521–1535.

Back, W., Hanshaw, B.B., Herman, J.S., Van Driel, J.N., 1986. Differential dissolution of a Pleistocene reef in the ground-water mixing zone of coastal Yucatan, Mexico. Geology 14, 137–140.

Bauer-Gottwein, P., Gondwe, B.R.N., Charvet, G., Marin, L.E., Rebolledo-Vieyra, M., Merediz-Alonso, G., 2011. Review: the Yucatan Peninsula karst aquifer, Mexico. Hydrogeol. J. 19, 507–524.

Beddows, P.A., 2004. Groundwater hydrology of a coastal conduit carbonate aquifer: Caribbean Coast of the Yucatan Peninsula, Mexico (Doctor of Philosophy: University of Bristol, 332 p.).

Beddows, P.A., Smart, P.L., Whitaker, F.F., Smith, S.L., 2007. Decoupled fresh-saline groundwater circulation of a coastal carbonate aquifer: spatial patterns of temperature and specific electrical conductivity. J. Hydrol. 346, 18–32.

Benavente, J., Hidalgo, M.c., Carrasco, F., April 2001. Influence of a high recharge episode following a drought period in an aquifer affected by seasonal seawater intrusion (Granada Coast S. Spain). Proceedings First International Conference on Saltwater Intrusion and Coastal Aquifers - Monitoring, Modeling and Management, Essaouira, Morocco, pp. 23–25.

Blaauw, M., 2010. Methods and code for "classical" age-modelling of radiocarbon sequences. Quat. Geochronol. 5, 512–518.
Brown, A.L., Reinhardt, E.G., van Hengstum, P.J., Pilarczyk, J.E., 2014. A coastal Yucatan sinkhole records intense hurricane events. J. Coast. Res. 30 (2), 418–428.
Coke, J., 1991. Sea-level curve. Nature vol. 353 (no. 5), 25.
Collins, S.V., Reinhardt, E.G., Rissolo, D., Chatters, J.C., Nava Blank, A., Luna Erreguerena, P., 2015. Reconstructing water level in Hoyo Negro, Quintana Roo, Mexico, implications for early Paleoamerican and faunal access. Quat. Sci. Rev. vol.124, 68–83 (in press).
Collins, S.V., Reinhardt, E.G., Werner, C.L., Meacham, S., Devos, F., LeMaillot, C., 2015. Regional response of the coastal aquifer to Hurricane Ingrid and sedimentation flux in the Yax Chen cave system (Ox Bel Ha) Yucatan, Mexico. Palaeogeogr. Palaeoclimatol. Palaeoecol. http://dx.doi.org/10.1016/j.palaeo.2015.07.030 (in press).
Esterson, K., 2003. Mixing Corrosion in a Coastal Aquifer (Masters of Science: Florida State University, 66 p.).
Finch, W.A., 1965. The Karst Landscape of Yucatan. University of Illinois, Urbana-Champaign.
Florea, L.J., Vacher, H.L., Donahue, B., Naar, D., 2007. Quaternary cave levels in peninsular Florida. Quat. Sci. Rev. 26, 1344–1361.
Gabriel, J.J., Reinhardt, E.G., 2006. Late Holocene (3500yBP) salinity changes and their climatic implications as recorded in an anchialine cave system, Ox Bel Ha, Yucatan, Mexico (Masters: McMaster University, 120 p.).
Gabriel, J.J., Reinhardt, E.G., Peros, M.C., Davidson, D.E., van Hengstum, P.J., Beddows, P.A., 2009. Palaeoenvironmental evolution of Cenote Aktun Ha (Carwash) on the Yucatan Peninsula, Mexico and its response to Holocene sea-level rise. J. Paleolimnol. 42, 199–213.
Hanshaw, B.B., Back, W., 1980. Chemical mass-wasting of the northern Yucatan Peninsula by groundwater dissolution. Geology 8, 222–224.
Hanstenrath, S., Greischar, L., 1993. Circulation mechanisms related to Northeast Brazil rainfall anomalies. J. Geophys. Res. 98 (D3), 5093–5102.
Hodell, D.A., Brenner, M., Curtis, J.H., Medina-Gonzalez, R., Ildefonso-Chan Can, E., Albornaz-Pat, A., Guilderson, T.P., 2005. Climate change on the Yucatan Peninsula during the Little Ice Age. Quat. Res. 63, 109–121.
Hughen, K.A., Overpeck, J.T., Peterson, L.C., Anderson, R.F., 1996. The nature of varved sedimentation in the Cariaco Basin, Venezuela, and it's paleoclimatic significance. Geol. Soc. Lond., Spec. Publ. 116, 171–183.
Kovacs, S.E., Gregory, B., 2013. Basal peat radiocarbon investigation. Unpublished raw data.
Lopez Fuerte, F.O., Siqueiros Beltrones, D.A., Navarro, J.N., 2010. Benthic diatoms associated with mangrove environments in the northwest region of Mexico. CICIMAR-Oceanides.
Lugo, A.E., Snedaker, S.C., 1974. The ecology of mangroves. Annu. Rev. Ecol. Syst. 5, 39–64.
Mazda, Y., Yokochi, H., Sato, Y., 1990. Groundwater flow in the Bashita-Minato mangrove area, and its influence on water and bottom mud properties. Estuar. Coast. Shelf Sci. 31, 621–638.
McKee, K.L., Cahoon, D.R., Feller, I.C., 2007. Caribbean mangroves adjust to rising sea level through biotic controls on change in soil elevation. Glob. Ecol. Biogeogr. 16 (5), 545–556.
Meacham, S.S., 2012. Using Landsat 5 TM Data to Identify and Map Areas of Mangrove in Tulum, Quintana Roo, Mexico (Masters of Science: University of New Hampshire, 105 p.).
Metcalfe, S.E., O'Hara, S.L., Caballero, M., Davies, S.J., 2000. Records of Late Pleistocene-Holocene climate change in Mexico—a review. Quat. Sci. Rev. 19, 699–721.
Milne, G.A., Peros, M., 2013. Data-model comparison of Holocene sea-level change in the circum-Caribbean region. Glob. Planet. Chang. 107, 119–131.
Moore, W.S., 1999. The subterranean estuary: a reaction zone of ground water and sea water. Mar. Chem. (no. 65), 111–125.
Moore, Y.H., Stoessell, R.K., Easley, D.H., 1992. Fresh-water sea-water relationship within a groundwater-flow system, northeastern coast of the Yucatan Peninsula. Ground Water 30 (3), 343–350.
Neuman, B.R., Rahbek, M.L., 2007. Modeling The Groundwater Catchment of the Sian Ka'an Reserve. National Speleological Society, Quintana Roo.
Peterson, L.C., Overpeck, J.T., Kipp, N.G., Imbrie, J., 1991. A high-resolution late Quaternary upwelling record from the anoxic Cariaco Basin, Venezuela. Paleoceanography 6, 99–120.
Pohlman, J.W., Iliffe, T.M., Cifuentes, L.A., 1997. A stable isotope study of organic cycling and the ecology of an anchialine cave ecosystem. Mar. Ecol. Prog. Ser. 155, 17–27.
Quintana Roo Speleological Survey, 2014. List of Long Underwater Caves in Quintana Roo. Tulum, Quintana Roo Speleological Survey, Mexico.
Raeisi, E., Mylroie, J.E., 1995. Hydrodynamic behaviour of caves formed in the fresh-water lens of carbonate islands. Carbonates Evaporites 10 (2), 207–214.
Reimer, P.J., Bard, M.G.L., Bayliss, A., Beck, J.W., Blackwell, P.G., Ramsey, C.B., Buck, C.E., Edwards, R.L., Freidrich, M., Groots, P.M., Guilderson, T.P., Haflidason, H., Hajdas, I., Hatté, C., Heaton, T.J., Hoffmann, D.L., Hogg, A.G., Hughen, K.A., Kaiser, K.F., Kromer, B., Manning, S.W., Nui, M., Reimer, R.W., Richards, D.A., Scott, E.M., Southon, J.R., Turney, C.S.M., van der Plicht, J., 2013. IntCal13 and Marine13 radiocarbon age calibration curves, 0-50,000 years Cal BP. Radiocarbon 55 (p. 1869-1887).
Schmitter-Soto, J.J., Comin, F.A., Escobar-Briones, E., Herrera-Silveira, J., Alcocer, J., Suarez-Morales, E., Elias-Gutierrez, M., Diaz-Arce, V., Steinich, B., 2002. Hydrogeochemical and biological characteristics of cenotes in the Yucatan Peninsula (SE Mexico). Hydrobiologia 467, 215–228.
Simon, K.S., Pipan, T., Culver, D.C., 2007. A conceptual model of the flow and distribution of organic carbon in caves. J. Cave Karst Stud. 69 (2), 279–284.
Smart, P.L., Beddows, P.A., Coke, J., Doerr, S., Smith, S., Whitaker, F.F., 2006. Cave development on the Caribbean coast of the Yucatan Peninsula, Quintana Roo, Mexico. In: Harmon, R.S.a.C.W. (Ed.), Perspectives on karst geomorphology, hydrology and geochemistry—A tribute volume to Derek C. Ford and William B. White. Geological Society of America Special Paper vol. 404, pp. 105–128.
Torrescano, N., Islebe, G.A., 2006. Tropical forest and mangrove history from southeastern Mexico: a 5000 yr pollen record and implications for sea level rise. Veget Hist Archaeobot 15 pp. 191–195.
Toscano, M.A., Macintyre, I.G., 2003. Corrected western Atlantic sea-level curve for the last 11,000 years based on calibrated ^{14}C dates from Acropora framework and intertidal mangrove peat. Coral Reefs 22, 257–270.
van Hengstum, P.J., Reinhardt, E.G., Beddows, P.A., Gabriel, J.J., 2010. Linkages between Holocene paleoclimate and paleohydrogeology preserved in a Yucatan underwater cave. Quat. Sci. Rev. 29 (19–20), 2788–2798.
van Hengstum, P.J., Scott, D.B., Grocke, D.R., Charette, M.A., 2011. Sea level controls sedimentation and environments in coastal caves and sinkholes. Mar. Geol. 286, 35–50.
van Hengstum, P.J., Richards, D.A., Onac, B.P., Dorale, J.A., 2015. Coastal caves and sinkholes. In: Shennan, Ian, Long, A.J., Horton, B.J. (Eds.), Handbook of Sea-Level Research. John Wiley and Sons Ltd.
Weidie, A.E., 1985. Geology of Yucatan Platform: Part 1 (19 p.).
Werner, C.L., 2007. Double-Diffusive Fingering in Porous Media (Doctor of Philosophy: Florida State University, 114 p.).
Wolanski, E., Mazda, Y., Ridd, P., 1992. Coastal and Estuarine Studies—Mangrove Hydrodynamics. American Geophysical UnionTropical Mangrove Ecosystems (329 p.).